


Experimental dynamic damage assessment of PUFJ protected brick infilled RC building during successive shake table tests

Arkadiusz KWIECIEŃ¹ , Zoran RAKICEVIC², Jarosław CHEŁMECKI¹, Aleksandra BOGDANOVIC², Marcin TEKIELI¹, Łukasz HOJDYS¹, Matija GAMS³, Piotr KRAJEWSKI¹, Filip MANOJLOVSKI², Antonio SOKLAROVSKI², Omer Faruk HALICI⁴, Theodoros ROUSAKIS⁵, and Vachan VANIAN⁵

¹ Faculty of Civil Engineering, Cracow University of Technology, Cracow, Poland

² IZIS, Ss. Cyril and Methodius University, Skopje, North Macedonia

³ Faculty of Civil and Geodetic Engineering, University of Ljubljana, Ljubljana, Slovenia

⁴ Istanbul Technical University, Istanbul, Turkey

⁵ Democritus University of Thrace, Xanthi, Greece

Abstract. It is highly important to determine eigenvalues before and after certain extreme events that may cause damage accumulation, such as earthquake, blasts and mining or seismic tests on research models. Unique experiment design and shake table testing was performed to investigate seismic performance of a 3D RC building model with infill walls and advanced protection with polyurethane-based joints and fiber polymer reinforced light and emergency jackets. For the purpose of wider experimental activities, three methods for determination of the dynamic characteristics were used during multiple successive shake table tests following a dynamic pushover approach, and they are presented in detail. They are: inertance function through impact hammer tests, standard Fourier transformation of measured acceleration time history and digital image correlation. The expected differences in the results are related to the type and intensity of excitation used, the involvement of materials with different mechanical and physical properties, and with the different rate and extent of damage accumulation, as well as to local or global measurements. Yet, all methods lead to reliable results when a consistent methodology is being used, that takes into account locality or globality of measurements, leaving a choice for the most suitable one, depending on the site conditions. The inertance function method presented manifested its high efficiency in analysis of dynamic properties of large-scale structures and in monitoring of their changes caused by the damage and repair process. It offers quite a wide range of useful information, does not require very expensive equipment and its transportation cost is negligible. This method seems to be a proper diagnostic tool for simple experimental modal analysis of real structures and their structural elements, where detection of changes in the structural condition and in dynamic properties is required, also as a non-destructive testing and monitoring method. Digital image correlation proved to be a promising non-contact tool, strongly supporting the conventional instrumentation of shake table testing, while the Fourier transformation was used as a benchmark method yielding the most reliable results.

Key words: shake table; earthquake; dynamic characteristics; modal hammer; DIC.

1. INTRODUCTION

Masonry structures, especially those of poor construction, are vulnerable to earthquakes. However, such structures are very popular around the globe because they are made of available cheap local materials, not requiring excessive funds. Moreover, the structures can be constructed by not highly qualified workers. The most popular vernacular masonry structures in such areas are stone masonry walls, earthen walls [1] or unreinforced brick masonry walls. One important consideration in ensuring protection and strengthening of massive masonries in seismic areas is the improvement of earthquake resistance of structures with strengthening systems carrying additional loads and in-

creasing structural ductility without increasing structural mass (the structure should be as light as possible).

Masonries are being damaged during earthquakes because of various reasons [2] due to generation of high inertial forces proportional to the mass of structure resulting from the action of seismic waves propagating through elastic soil supporting the structures. The magnitude of the inertial forces increases proportionally to the weight of structures and resonance. The resultant stresses (hazardous for masonries: shear, tensile) accumulate rapidly as the duration of the vibration increases, aggravating the structural damage. Damage process causes changes in structural stiffness, dangerous especially in the resonance zone of the dynamically excited structure. It is mainly affected by the cyclic nature of dynamic loads, acting with dominant frequency band characteristic for the seismic area, when they are close to resonance [3]. Seismic loads, in most cases, generate stresses that exceed the strength of the brittle masonry build-

*e-mail: akwiecie@pk.edu.pl

Manuscript submitted 2022-09-30, revised 2023-01-16, initially accepted for publication 2023-02-13, published in June 2023.

ing materials. Deterioration process of the masonry materials starts even at a relatively low load level, with appearance of stress concentrations in places of material discontinuities .. [4]. Under the peak of stress concentration, brittle materials easily reach their limit of elasticity and start fracturing. Stress concentrations cause damages in masonry structures at low load level especially when they are of poor construction. The huge mass of construction material and low strength lead to massive disasters during earthquakes [5].

During rapid visual screening of the structural condition of structures, the damage pattern usually allows engineers to roughly evaluate its safety, detect the main reasons of observed damages and deformations, and suggest further inspections or repairs, or determine full functionality [6–8]. In most cases, especially those related to historical structures, rapid visual screening concludes roughly the extent and depth of additional exhaustive inspections [9]. In such cases, more or less complicated diagnosis tools (laboratory and in situ tests on material properties, geometry survey, dynamic and foundation investigation, or analysis of numerical models) are used and a large team of various experts may be engaged (in very complex cases). Especially in historical structures, knowledge about past reconstructions and structural interventions is critical. There an expert has to behave like a detective to discover real danger and needs requiring a proper structural intervention [9]. Often, the bad structural condition of the analyzed structure remains unknown and sudden collapse without any warning occurs, as in the case of the Pavia Civil Tower in Italy [10]. That is why monitoring of structural condition of heritage [11, 12] and civil engineering structures [13, 14] is required.

Hidden structural damage and the resulting change in stiffness are difficult to detect without dynamic investigation. The new diagnosis approach based on inertance and compliance functions [15–17] is presented, which allows for detecting changes in eigenfrequency and thus in global or local structural stiffness. This information is significant when structural eigenfrequencies start to be close to the dominant frequency band characteristic for a seismic area [3]. The resonance threat, assessed during dynamic monitoring of a structure, should trigger

a structural intervention process to avoid sudden collapse of urban and heritage structures during the next earthquake. The presented diagnostic methodology allows also for determining the damping of the structure [18], which together with the natural frequencies can also be useful for validation of numerical models of structures. Properly validated numerical models [19, 20] allow engineers to easily assess the vulnerability and stability of analyzed structures. This diagnosis methodology is presented on structural examples but also compared with the traditional Fourier transformation from selected acceleration time histories as well as with the digital image correlation technique.

The present study is based on experimental results of the “INfills and MASONry structures protected by deformable POLyurethanes in seismic areas” (INMASPOL) project within the SERA, Horizon 2020. This project investigates, in several phases, the seismic performance of a system consisting of a reinforced concrete frame and infill with thermally isolated bricks [21] in a seismic table. Two innovative structural interventions are provided to the system to successfully ensure its integrity, especially the infill in in-plane and out-of-plane seismic excitations. The first involves the application of polyurethane seismic joints (PUFJ) at the frame-infill interface to increase the energy dissipation capacity while reducing damage accumulation. The second is an emergency repair system [22] consisting of a glass fiber grid bonded with polyurethane (FRPU) to the weak masonry substrate, with the main objective of preventing the disintegration of weak masonry during the aftershocks.

2. METHODOLOGY AND DESCRIPTION OF EXPERIMENTALLY DETERMINED STRUCTURAL CHARACTERISTICS

Within the framework of the H2020 SERA project, a real scale 3D specimen, consisting of a RC frame with infill walls protected by PUFJ and FRPU systems, was tested dynamically on a shake table at the IZIIS laboratory in Skopje, North Macedonia. The specimen is presented in Fig. 1 while the setup and specimen details are presented in [23].

The model was tested in 4 phases. Symmetrically built infill walls of type B (3 injected PUFJ interfaces) and type C

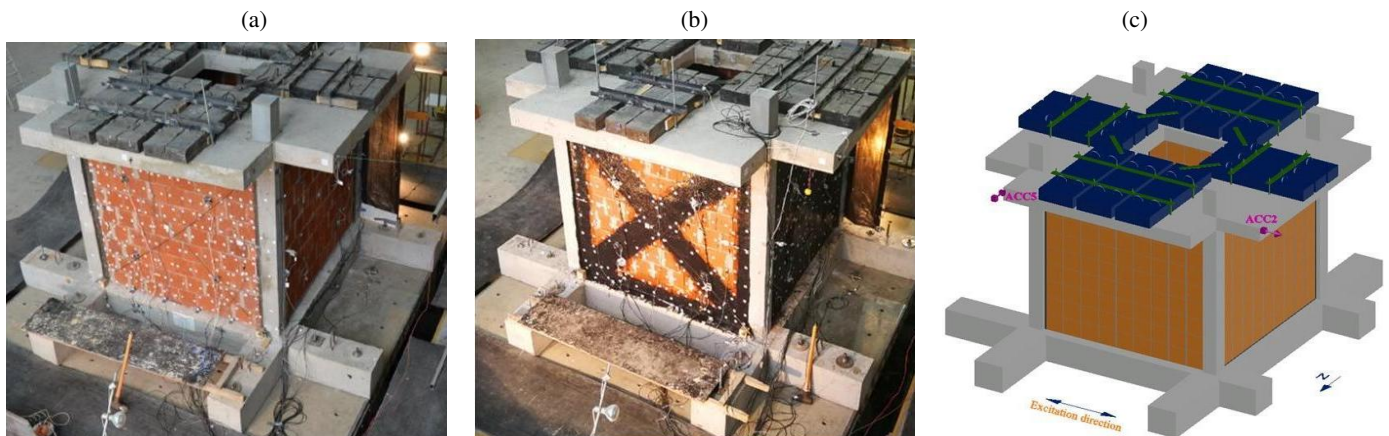


Fig. 1. View of the RC building with infill walls protected by PUFJ and FRPU on the shake table at IZIIS: (a) specimen tested in phase 1 and 2, (b) specimen tested in phase 3 and 4, (c) test model and location of accelerometers 2 and 5

(4 prefabricated PUFJ interfaces) were tested in-plane and out-of-plane simultaneously [23]. The seismic excitations followed the scaled Kefalonia 2014 earthquake, up to 77% of its maximum intensity (EQ90%). The seismic excitations were accompanied by white noise and impact hammer excitations and are presented in application order in Table 1 and Table 2 for all 4 testing phases.

Table 1
Tests performed. First part – 1 and 2

Phase	Test No.	Name	Type of excitation
PHASE 1	1–16	Hammer 1–16	Impact hammer
	17	Test 1	White noise
	18	Test 2	White noise
	20–22	Test 4	EQ 5%; 10%; 20%
	23	Test 7	White noise
	24–32	Hammer 17–24	Impact hammer
	33–34	Test 8	EQ 40%; 60%
	35	Test 10	White noise
	36	Test 11	EQ 80%
	37	Test 12	White noise
	38	Test 13	EQ 90%
	39	Test 14	White noise
	40–55	Hammer 25–40	Impact hammer
	56	Test 15	EQ 90% stopped
	57	Test 16	White noise
	58	Test 17	EQ 80%
	59	Test 18	White noise
	60	Test 19	EQ 90%
	61–70	Hammer 41–50	Impact hammer
	PHASE 2	71–86	Hammer 51–66
87		Test 20	White noise
91–93		Test 24	EQ 10%; 20%; 30%
94		Test 27	White noise
95–110		Hammer 67–82	Impact hammer

In phase 1, the infill walls of type B were tested in-plane and the infill walls of type C were tested out-of-plane. In phase 2, the heavily damaged B-type walls were strengthened with FRPU on both sides (B_FRPU). Then, the 3D specimen was excited again up to EQ30% to avoid collapse of the structure and thus, secure it for the next phases of the tests. In phase 3, the building was rotated by 90 degrees. Type C walls were tested in-plane up to EQ30% as the bonds in the mortar joints between the infill wall blocks started to disintegrate. In the same phase, B_FRPU specimens were tested out-of-plane. In phase 4, after the FRPU strengthening of the type C walls (C_FRPU), the tests continued up to EQ70%.

Table 2
Tests performed. Second part – 3 and 4

Phase	Test No.	Name	Type of excitation
PHASE 3	111–126	Hammer 83–98	Impact hammer
	127	Test 28	White noise
	128	Test 29	EQ 10%
	129	Test 30	White noise
	130	Test 31	EQ 20%
	131	Test 32	White noise
	132–147	Hammer 99–114	Impact hammer
	148	Test 33	EQ 30%
	149	Test 34	White noise
	150–165	Hammer 115–130	Impact hammer
PHASE 4	166–181	Hammer 131–146	Impact hammer
	182	Test 35	White noise
	183	Test 36	EQ 10%
	184	Test 37	White noise
	185	Test 38	EQ 20%
	186	Test 39	White noise
	187	Test 40	EQ 30%
	188	Test 41	White noise
	189	Test 42	EQ 40%
	190	Test 43	White noise
	191	Test 44	EQ 50%
	192	Test 45	White noise
	193–208	Hammer 147–162	Impact hammer
	209	Test 46	EQ 60%
	210	Test 47	White noise
	211	Test 48	EQ 70%
	212	Test 49	White noise
	213	Hammer 163–178	Impact hammer

3. THEORETICAL BACKGROUND OF INERTANCE FUNCTION ASSESSMENT

The inertance function $I(\omega)$ is defined as quotient of frequency characteristics of measured acceleration $a(\omega)$ and excitation force $F(\omega)$, in angular frequency domain ω (in radian/second).

Alternatively, frequency domain f (in Hertz) relates the frequency characteristics of measured acceleration $a(f)$ and excitation force $F(f)$, based on the well-known $\omega = 2\pi f$.

In practice, it is more convenient to use the modulus of both frequency characteristics. The quotient of the modulus of the frequency characteristics mentioned above provides the modulus of the inertance function (Fig. 2). Definitions of other useful moduli of frequency characteristics such as: apparent mass $M(\omega)$, dynamic stiffness $D(\omega)$, compliance function $A(\omega)$, inertial force $F'(\omega)$, dynamic displacement $X(\omega)$ and potential energy $E_p(\omega)$, are presented in Fig. 2.

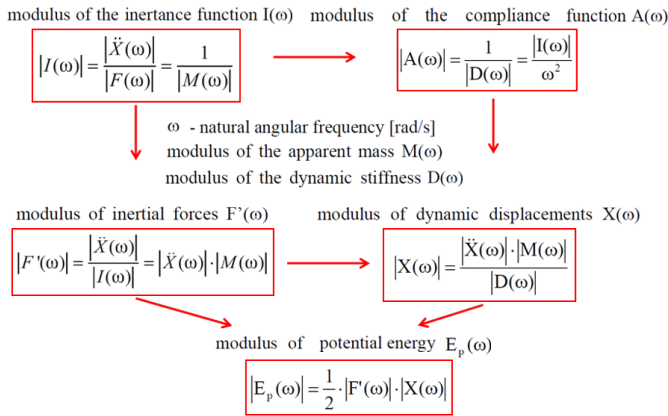


Fig. 2. Useful functions calculated from frequency characteristics of excitation force $F(\omega)$ and acceleration $a(\omega)$

Dynamic diagnosis tests with the use of the inertance function require special equipment for dynamic measurements. They involve a modal hammer (Fig. 3a) – registering im-

pulse excitation force F in the time domain, an accelerometer (Fig. 3b) – registering acceleration response of an excited structure in the time domain, and a recorder acquiring and analyzing the data with the use of the fast Fourier transform (Fig. 3c). Obtained frequency characteristics of excitation force and measured acceleration are used to define the inertance function. Stiffness and damping changes based on impact diagnosis with a modal hammer are presented henceforth, followed by two practical applications of the same method. Example inertance and compliance functions determined for the whole 3D RC building with PUFJ protected brick infills and for the brick infill wall with local dynamic characteristics are presented in Fig. 4b, 4c and 5b, 5c, respectively.

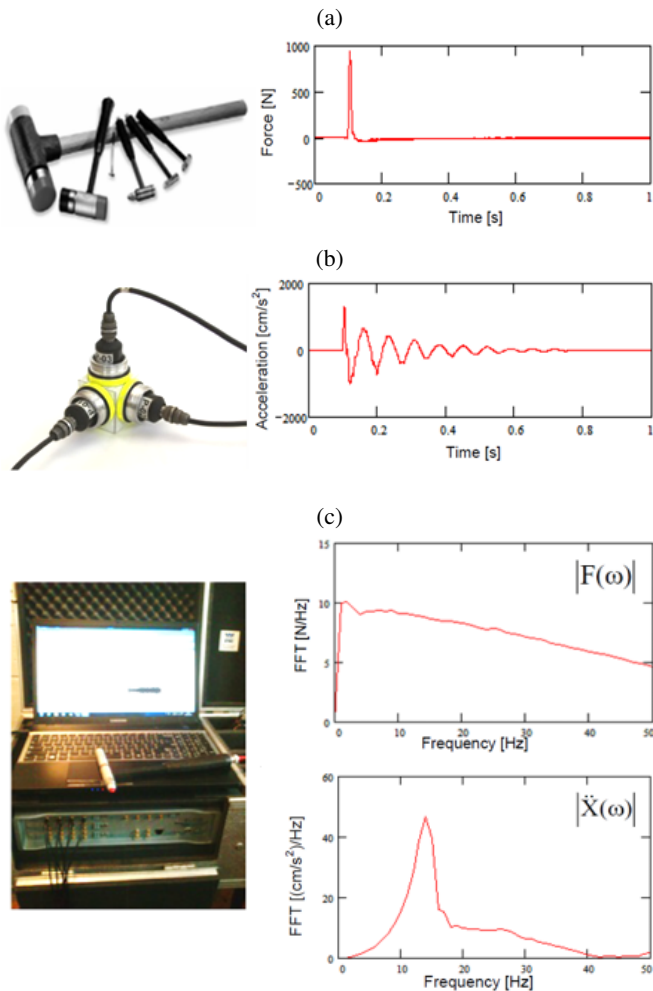


Fig. 3. Measurement equipment and results: modal hammers and force response in time domain (a), accelerometers and acceleration response in time domain (b), acquisition system with modal analysis and calculated frequency characteristics of excitation force and measured acceleration (c)

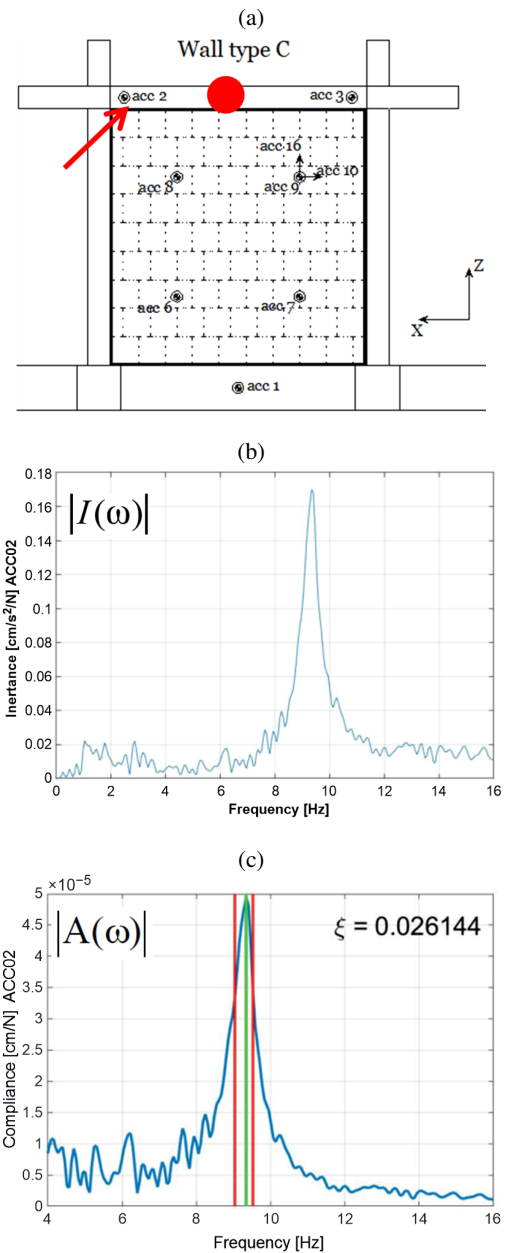


Fig. 4. Location of a hitting point and receiving accelerometer (a), determined inertance function (b) and compliance function with damping ratio calculated by the half-power band width method (c)

Experimental dynamic damage assessment of PUFJ protected brick infilled RC building during successive shake table tests

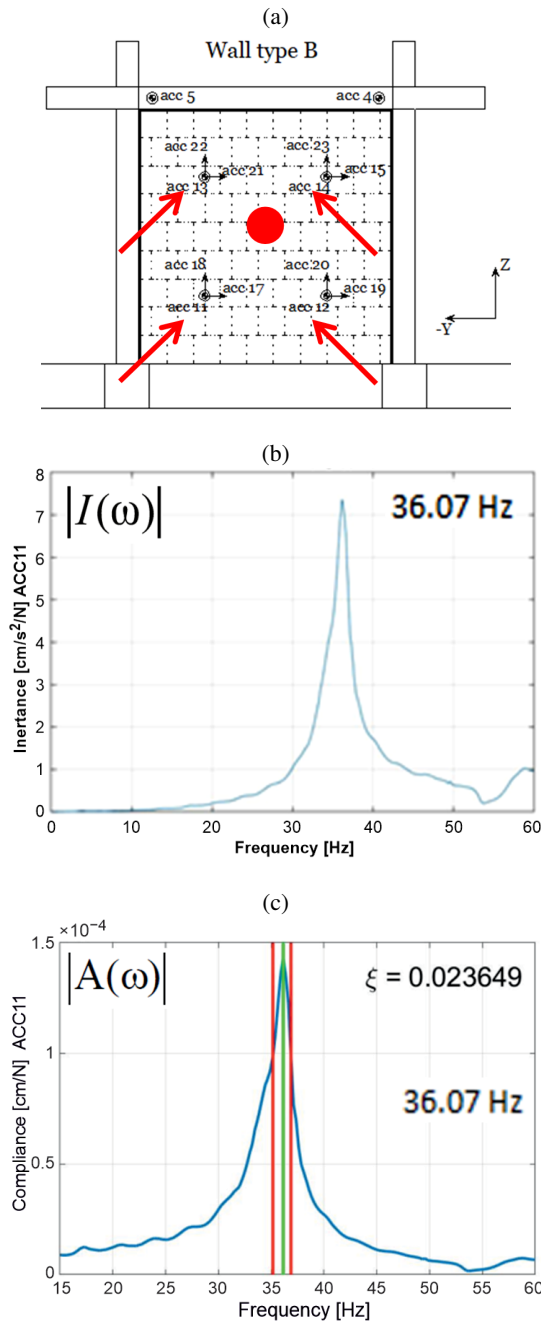


Fig. 5. Location of a hitting point and receiving accelerometers on an infill wall (a), determined example inertance function (b) and compliance function with damping ratio calculated by the half-power band width method (c)

3.1. Stiffness and damping changes of PUFJ protected structure based on impact diagnosis with modal hammer

A modal hammer of 5 kg in mass and accelerometers installed on the RC frame and on brick infill walls (Fig. 4a and 5a) were used for determination of the inertance and compliance functions. The whole 3D building’s dynamic response was acquired by acc. 2 on an RC slab when the impact excitation was realized in the middle of the slab (see red dot in Fig. 4a). The infill wall’s out-of-plane dynamic response was acquired by 4 accelerome-

ters when the impact excitation was realized in the middle of the wall (see red dot in Fig. 5a). The sequence of hammer impact excitations before and after seismic excitations of the structure on the seismic table is presented in Table 1 and 2.

Discussion of results obtained with this method is presented for phase 1, for the following impact tests: Hammer 1–16 before seismic testing; 17–24 after seismic excitation up to EQ30% and structure drift (top slab displacement divided by the structure height) of 0.27%; 25–40 after seismic excitation up to EQ90% and structure drift of 1.33% and 41–50 after another 3 seismic excitations up to EQ90% and structure drift of 3.7% (Table 1 and [23]).

Under hammer impact excitations, the following dominant frequencies were determined using acc. 2: 9.3 Hz, 8.1 Hz, 6.0 Hz and 1.8 Hz. The first 3 frequencies are higher than the dominant frequencies determined by white noise (Tests: 2, 7 and 14): 6.9 Hz, 6.8 Hz and 5.0 Hz due to lower excitation energy provided by the modal hammer than the shake table and thus stiffer dynamic response in the first case.

Higher difference in the last measured frequencies (1.8 Hz vs. 4.0 Hz) is due to diagnosis testing carried out before serious damages of infills B at the end of phase 1 (Test 19) – white noise, and after Test 19 – with the modal hammer, when the 3D building significantly lost its global stiffness for drift of structure equal to 3.7%.

Diagrams in Fig. 6 compare global stiffness and damping of the whole 3D building model and the infill wall before and after damage in phase 1, using the stiffness and damping ratio normalized to the values determined before phase 1. Changes of global stiffness of the 3D building and of the infill wall are presented in Fig. 6a and 6c, respectively, based on the inertance

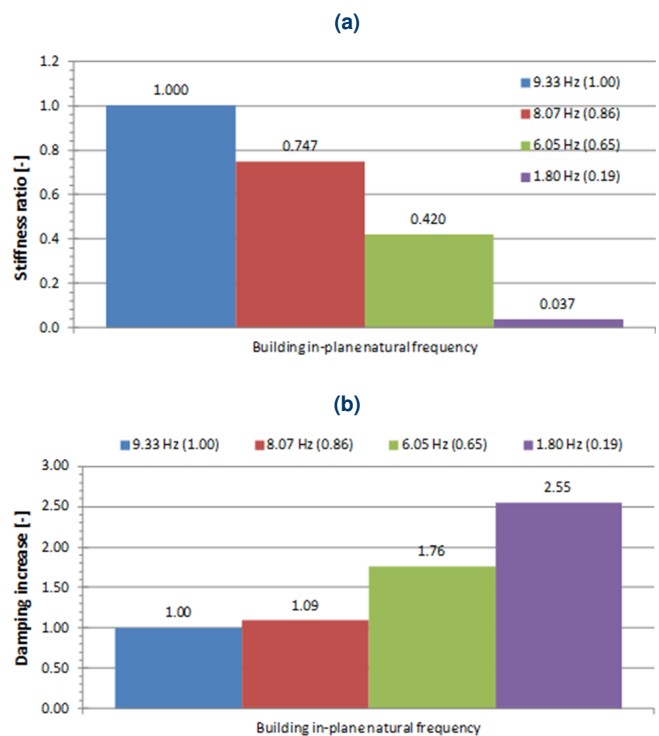


Fig. 6 (a), (b)

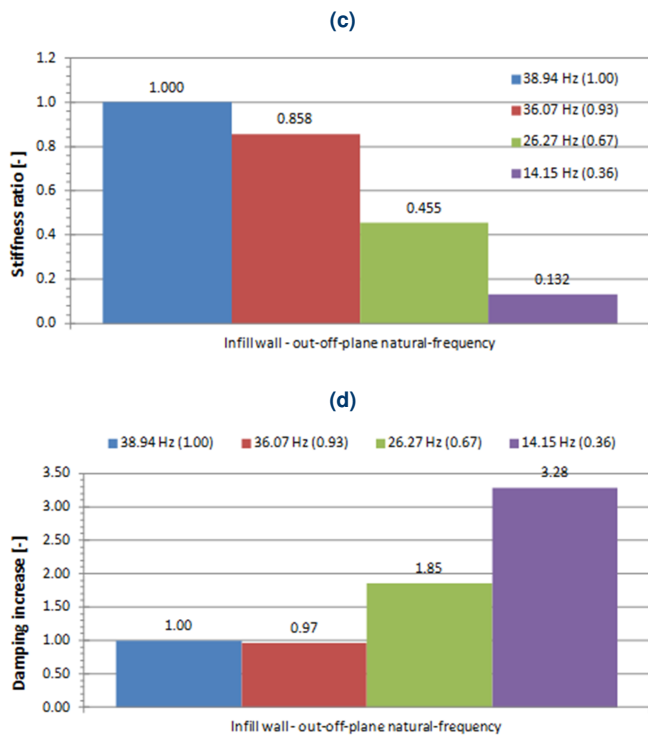
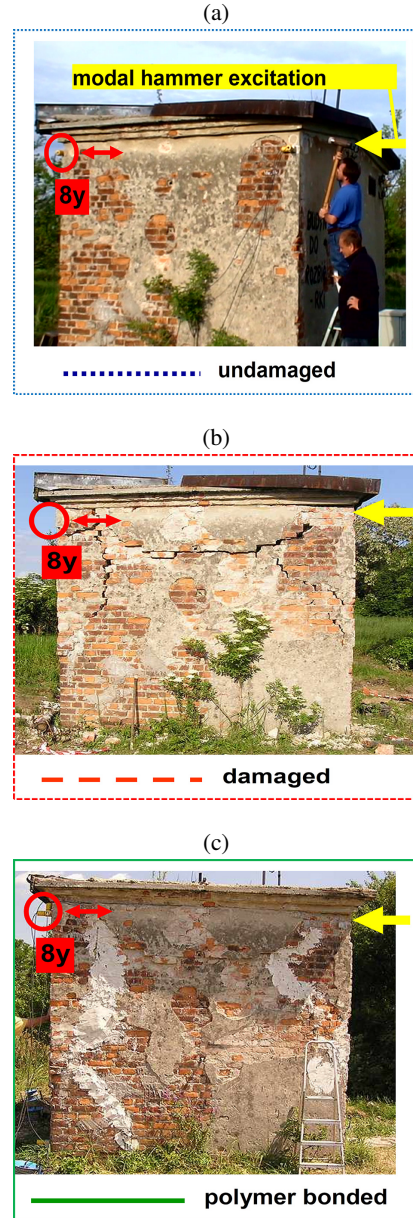


Fig. 6. Comparison of global stiffness and damping of the whole 3D building model and the infill wall before and after damage in phase 1, using the stiffness and damping ratio normalized to the values determined before phase 1. Stiffness ratio changes of the whole 3D building (a), corresponding damping ratio changes (b), stiffness ratio changes of the infill wall (c) and corresponding damping ratio changes (d), related to dominant frequencies with related frequency change ratios



functions. The compliance functions allowed for calculation of damping ratio values in phase 1 for the 3D building and for the infill wall. These variations of the values are presented in Fig. 6b and 6d, respectively.

3.2. Practical application of the inertance function – diagnosis of a small masonry building

The second example of using the inertance function is presented on a masonry building damaged artificially by a hit of an excavator bucket and repaired with polyurethane flexible joints [24] – Fig. 7.

Dynamic diagnosis of the building dynamic properties was carried out on an undamaged building (stage 1 – Fig. 7a), a damaged building (stage 2 – Fig. 7b) and a repaired one (stage 3 – Fig. 7c) using the 5kg modal hammer impulse excitation and a system of accelerometers installed on the tested building. Analysis is presented for one horizontal accelerometer response (8y).

Inertance functions in the frequency domain (Fig. 7d) were determined for stage 1 (blue line), stage 2 (red line) and stage 3 (green line). When the building underwent serious damage, the inertance function amplitude increased and its peak shifted into lower frequencies, which corresponded to building stiffness and inertial forces decrease. When the building was re-

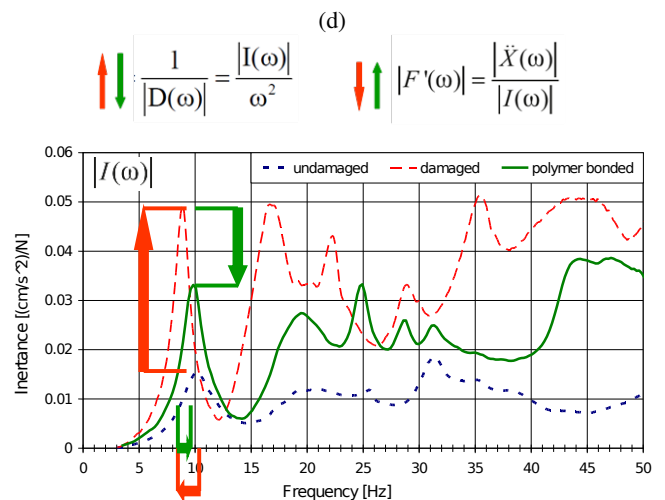


Fig. 7. Dynamic diagnosis of a small masonry building using inertance functions

paired with polyurethane flexible joints (injection into cracks), the inertance function amplitude decreased and its peak shifted into higher frequencies, which corresponded to building stiffness and inertial forces increase (Fig. 7d).

The compliance function derived from the inertance function (Fig. 2) allows for calculating the damping ratio ξ using the half-power bandwidth method (Fig. 8). Changes of damping in the tested building were determined for 3 analyzed stages (Fig. 7a–7c) and compared. Damping decreased when the building underwent damage, and increased after repair.

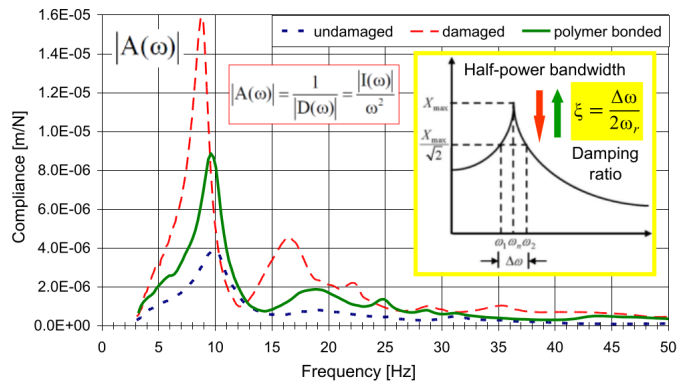


Fig. 8. Determination of damping ratio from the compliance function for 3 analyzed stages of the building

Damping was calculated also for higher eigenfrequencies of the analyzed 3 stages of the building, visible in the compliance functions (Fig. 8), from which functions of the equivalent Rayleigh damping can be drawn graphically (Fig. 9) and used in a numerical approach for model calculations [24].

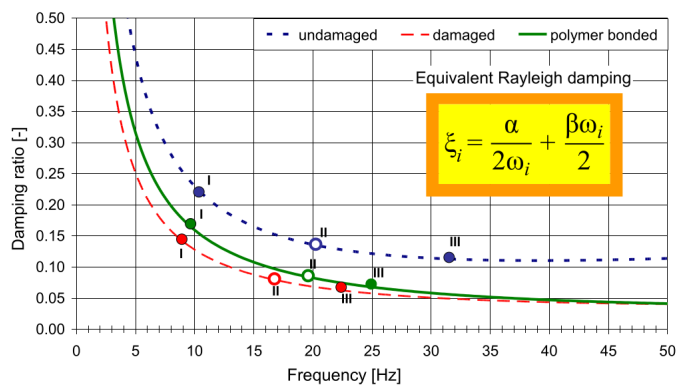


Fig. 9. Functions of equivalent Rayleigh damping, presented based on damping ratio values calculated for the first three eigenfrequencies of the analyzed stages, visible in the inertance functions – useful for the numerical approach to model calculations

4. STRUCTURAL DYNAMIC CHARACTERISTICS DETERMINED BY FOURIER TRANSFORMATION

Whenever a structural model is being tested on shake table to determine its earthquake response, it is very common that after certain levels of excitations the change of dynamic properties is

being observed, mainly due to global stiffness changes. Usually, this is done by means of low intensity excitation tests of white noise from which the eigenfrequencies can be easily determined with use of simple Fourier transform.

Table 1 and Table 2 show that the white noise excitations were applied after almost all earthquake tests in all test phases. On average, white noise excitations had input frequency range of 1–45 Hz and acceleration of 0.02g.

Since the tested model was fully symmetrical, only the results from both perpendicular walls are presented henceforth, i.e. accelerometers 2 and 5 (Fig. 1c). The graphical comparison of FFT shown in Fig. 10–11 is divided into 4 parts, following the testing phases.

The peaks of the plots clearly denote the dominant frequencies in the direction of the wall where the accelerometer was placed. Tables 3 and 4 show the dominant frequency values numerically where the trend of change toward lower frequencies with building stiffness loss and toward higher frequencies with building stiffness increase is evident.

Table 3

Eigenfrequencies obtained by FFT. First phase – 1 and 2

Phase	Test	Accelerometer	Frequency [Hz]
PHASE 1	Test 2	2	6.9
		5	6.9
	Test 7	2	6.8
		5	6.8
	Test 10	2	6.6
		5	6.6
	Test 12	2	6.3
		5	6.3
	Test 14	2	5.0
		5	5.8
Test 16	2	5.1	
	5	6.0	
Test 18	2	4.0	
	5	5.45	
PHASE 2	Test 20	2	3.60
		5	4.8
	Test 27	2	2.55
		5	4.2

The data presented in Tables 3 and 4 are utilized to calculate changes of global stiffness of the building based on equation (1). Parameters f_0 and f_n are measured initial and current eigenfrequencies, and EI_0 and EI_n are global initial and current stiffness of the building, respectively.

$$(EI_n)/(EI_0) = \frac{(f_n)^2}{(f_0)^2} \quad (1)$$

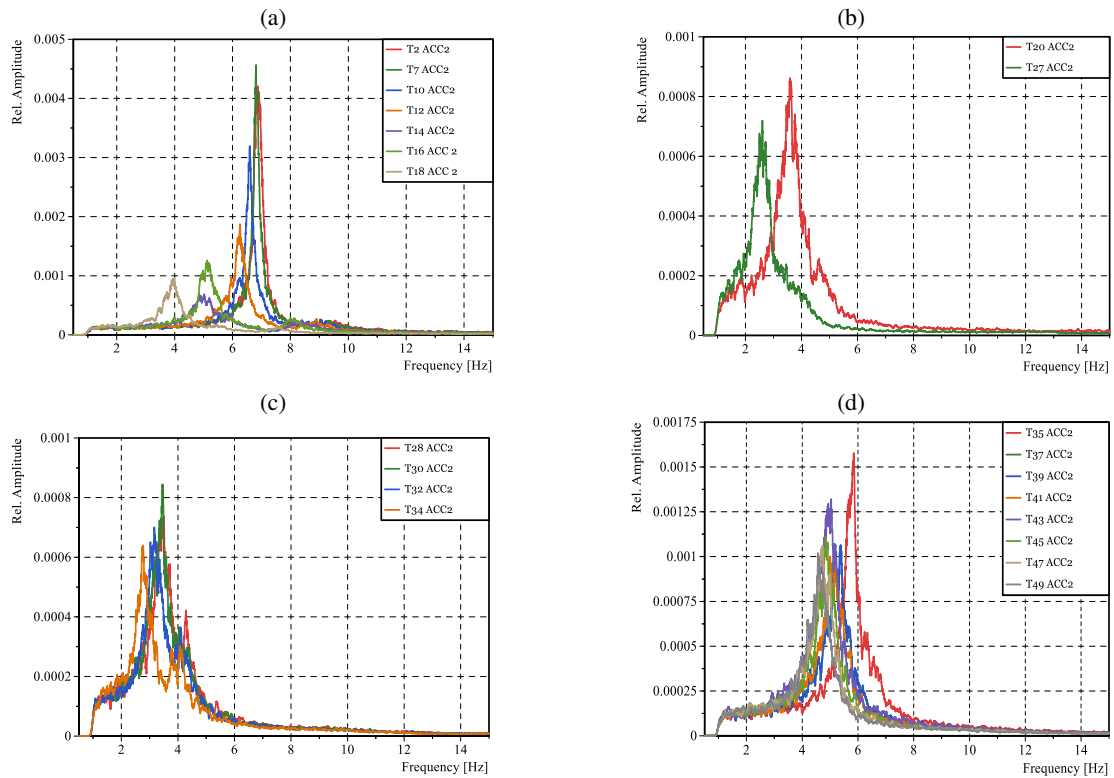


Fig. 10. FFT plots of ACC 2 (in excitation direction Y): tests 2, 7, 10, 12, 14, 16 and 18 (infill B in-plane, infill C out-of-plane) in phase 1 (a), tests 20 and 27 (infill B_FRPU in-plane, infill C out-of-plane) in phase 2 (b), tests 28, 30, 32 and 34 (infill C in-plane, infill B_FRPU out-of-plane) in phase 3 (c), tests 35, 37, 39, 41, 43, 45, 47 and 49 (infill C_FRPU in-plane, infill B_FRPU out-of-plane) in phase 4 (d)

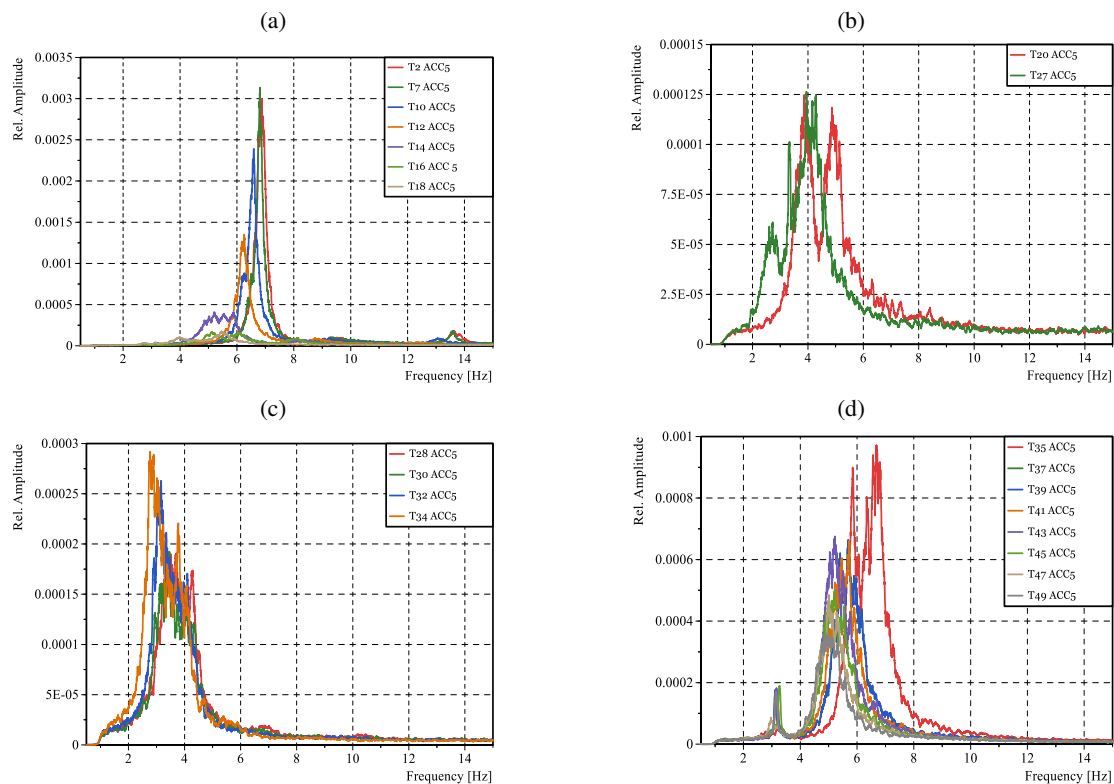


Fig. 11. FFT plots of ACC 5 (in direction X – perpendicular to excitation direction Y): tests 2, 7, 10, 12, 14, 16 and 18 (infill B in-plane, infill C out-of-plane) in phase 1 (a), tests 20 and 27 (infill B_FRPU in-plane, infill C out-of-plane) in phase 2 (b), tests 28, 30, 32 and 34 (infill C in-plane, infill B_FRPU out-of-plane) in phase 3 (c), tests 35, 37, 39, 41, 43, 45, 47 and 49 (infill C_FRPU in-plane, infill B_FRPU out-of-plane) in phase 4 (d)

Table 4

Eigenfrequencies obtained by FFT. First phase – 3 and 4

Phase	Test	Accelerometer	Frequency [Hz]
PHASE 3	Test 28	2	3.5
		5	3.5
	Test 30	2	3.45
		5	3.45
	Test 32	2	3.2
		5	3.15
Test 34	2	2.75	
	5	2.85	
PHASE 4	Test 35	2	5.8
		5	6.6
	Test 37	2	5.4
		5	5.7
	Test 39	2	5.4
		5	5.7
	Test 41	2	5.0
		5	5.7
	Test 43	2	5.0
		5	5.2
	Test 45	2	4.9
		5	5.2
Test 47	2	4.7	
	5	5.0	
Test 49	2	4.6	
	5	4.9	

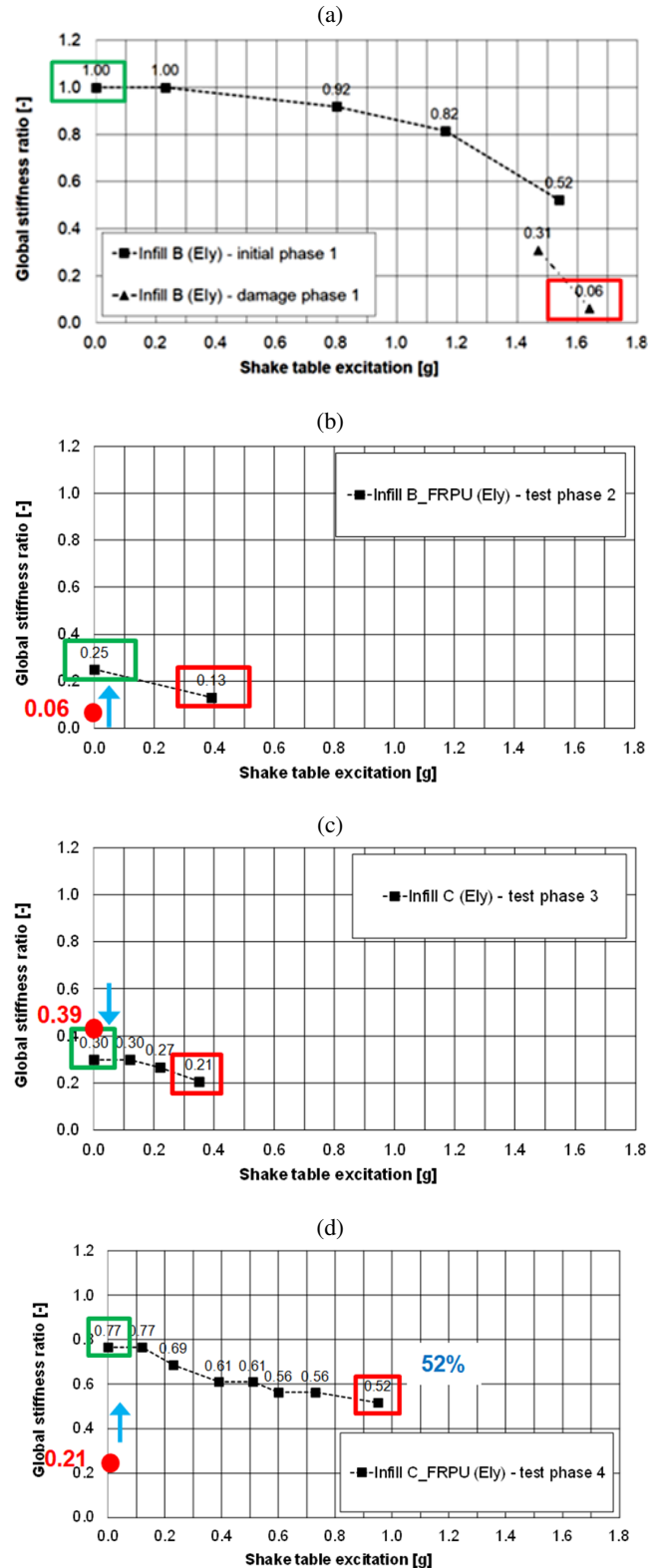


Fig. 12. Global stiffness changes in excitation direction Y: tests 2, 7, 10, 12, 14, 16 and 18 (infill B in-plane) in phase 1 (a), tests 20 and 27 (infill B_FRPU in-plane) in phase 2 (b), tests 28, 30, 32 and 34 (infill C in-plane) in phase 3 (c), tests 35, 37, 39, 41, 43, 45, 47 and 49 (infill C_FRPU in-plane) in phase 4 (d). Green frame – initial value in the current phase; Red frame – final value in the current phase; Red dot – final value from the previous phase; Blue arrow – increase/decrease of the values during phases' change

Following the change, in the initial phase when the walls were not repaired, the drop of the value of the eigenfrequency is clearly large for the in-plane excited wall and differs from the out-of-plane excited wall for accelerometers 2 and 5, respectively. Once the walls were repaired by means of FRPU bonded to the walls, the stiffness of the walls improved significantly and affected the overall performance of the structure, also in the frequency domain. Detailed elaboration of the method itself is given in [23].

Fig. 12–13 present changes of stiffness in testing phases 1–4, related to the direction of excitation (Y) and the direction perpendicular to the direction of excitation (X).

In phase 1, after 10 series of shaking up to EQ90%, the global stiffness ratio was reduced from 1 to 0.06 in Y direction for infills B and to 0.39 in X direction for infills C (Fig. 12a and 13a). In phase 2, strengthening of seriously cracked infills B with FRPU caused visible increase of the global stiffness ratio, from 0.06 to 0.25 in Y direction, and negligible change from 0.39 to 0.37 in X direction (Fig. 12b and 13b).

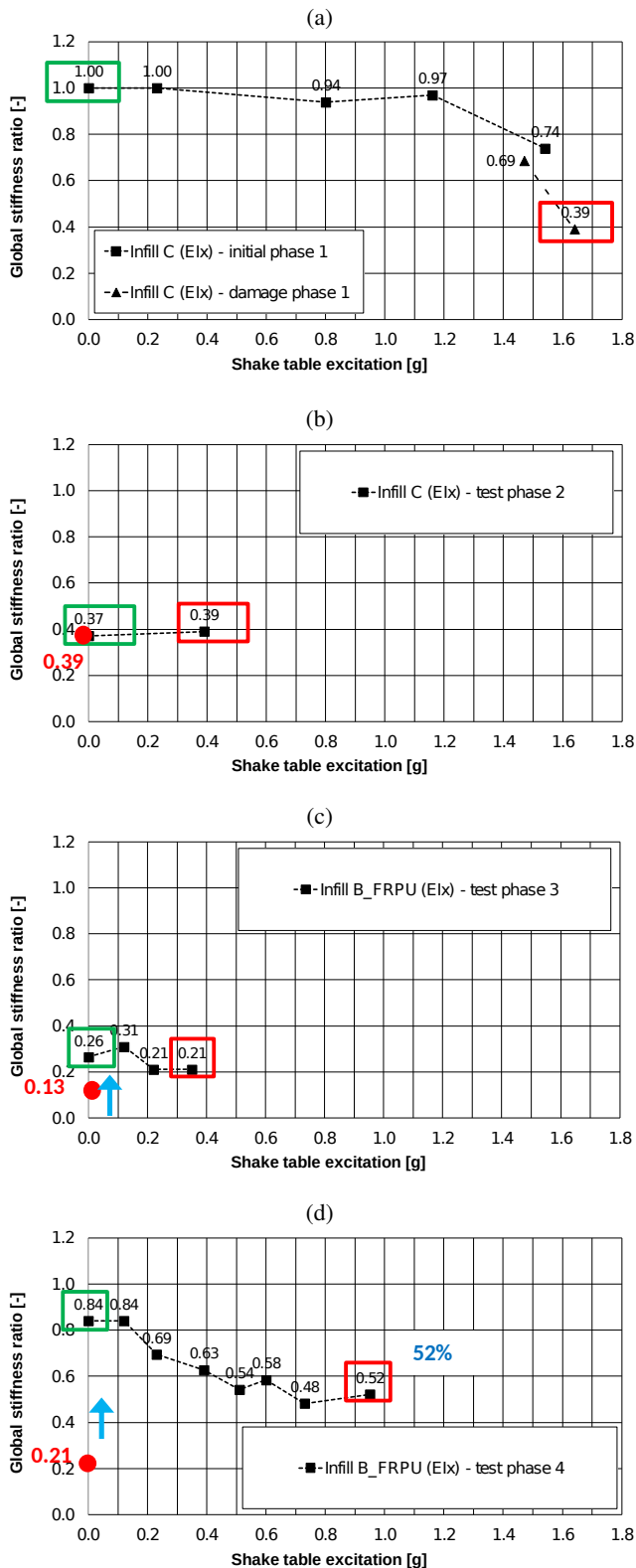


Fig. 13. Global stiffness changes in direction X, perpendicular to excitation direction Y: tests 2, 7, 10, 12, 14, 16 and 18 (infill B in-plane) in phase 1 (a), tests 20 and 27 (infill B_FRPU in-plane) in phase 2 (b), tests 28, 30, 32 and 34 (infill C in-plane) in phase 3 (c), tests 35, 37, 39, 41, 43, 45, 47 and 49 (infill C_FRPU in-plane) in phase 4 (d). Green frame – initial value in the current phase; Red frame – final value in the current phase; Red dot – final value from the previous phase; Blue arrow – increase/decrease of the values during phases’ change

After 3 series of shaking up to EQ30%, the global stiffness ratio was reduced from 0.25 to 0.13 in Y direction for infills B_FRPU and changed from 0.37 to 0.39 in X direction for infills C (Fig. 12b and 13b, respectively).

The specimen was next rotated by 90 degrees, thus infills B_FRPU were tested out-of-plane and infills C were tested in-plane. This process slightly changed the initial parameters after rotation. The global stiffness ratio decreased from 0.39 to 0.30 in Y direction for infills C and increased from 0.13 to 0.26 in X direction for infills B_FRPU (Fig. 12c and 13c).

In phase 3, after 3 series of shaking up to EQ20%, the global stiffness ratio was reduced from 0.30 to 0.21 in Y direction for infills C and from 0.26 to 0.21 in X direction for infills B_FRPU (Fig. 12c and 13c, respectively).

The test was stopped due to visible plastic hinges at tops and bottoms of columns, bed mortar joints opening and low global stiffness of the specimen, which was in danger of collapsing. In this phase, infills C were decided to be strengthened with FRPU solution (Fig. 1b).

Phase 4 was effected after infills C were strengthened with FRPU. This action caused significant increase of the global stiffness ratio, from 0.21 to 0.77 in Y direction and from 0.21 to 0.84 in X direction (Fig. 12d and 13d, respectively). Such large changes in stiffness indicate very high efficiency of the FRPU applied in recovery of structural safety. After 7 series of shaking up to EQ50% in phase 4, the global stiffness ratio was reduced from 0.77 to 0.52 in Y direction for infills C_FRPU and from 0.84 to 0.52 in X direction for infills B_FRPU (Fig. 12d and 13d, respectively). The experimental campaign was stopped due to the actuator limit state of the shake table and the impossibility of testing continuation. The maintained stiffness of the 3D specimen in both directions X and Y at the level of 52% indicates that the RC frame structure with infill walls protected by PUFJ and FRPU is able to withstand further serious dynamic loading. This was confirmed by a further testing campaign carried out on this not-collapsed specimen using forced harmonic vibration tests in resonance. The tested structure survived, without collapse, the excitations lasting for a total period of over 2 hours with max. acc. = 0.77 g, max. disp. = 30.15 mm and max. drift = 1.3% [25].

5. DIGITAL IMAGE CORRELATION – DIC

The digital image correlation method was applied in the tests to assess the performance of PUFJ interface connecting an RC frame and an infill wall during earthquake excitation on a shake table. This method captures the variation of large deformations of flexible connections over time, using a photo camera and CivEng Vision software [26]. Before the acquisition process, special markers were bonded on the testing surface (Fig. 14a) on both sides of the PUFJ connection. Figures 14b and 14c present horizontal and vertical relative displacement over time between the upper and bottom boundary of the PUFJ, registered for shake table excitation with 1.56 g, and accompanying drift of the structure of 1.21%.

In the horizontal graph (Fig. 14b), the characteristic variation of relative displacements due to the “Kefalonia earthquake”-

Experimental dynamic damage assessment of PUFJ protected brick infilled RC building during successive shake table tests

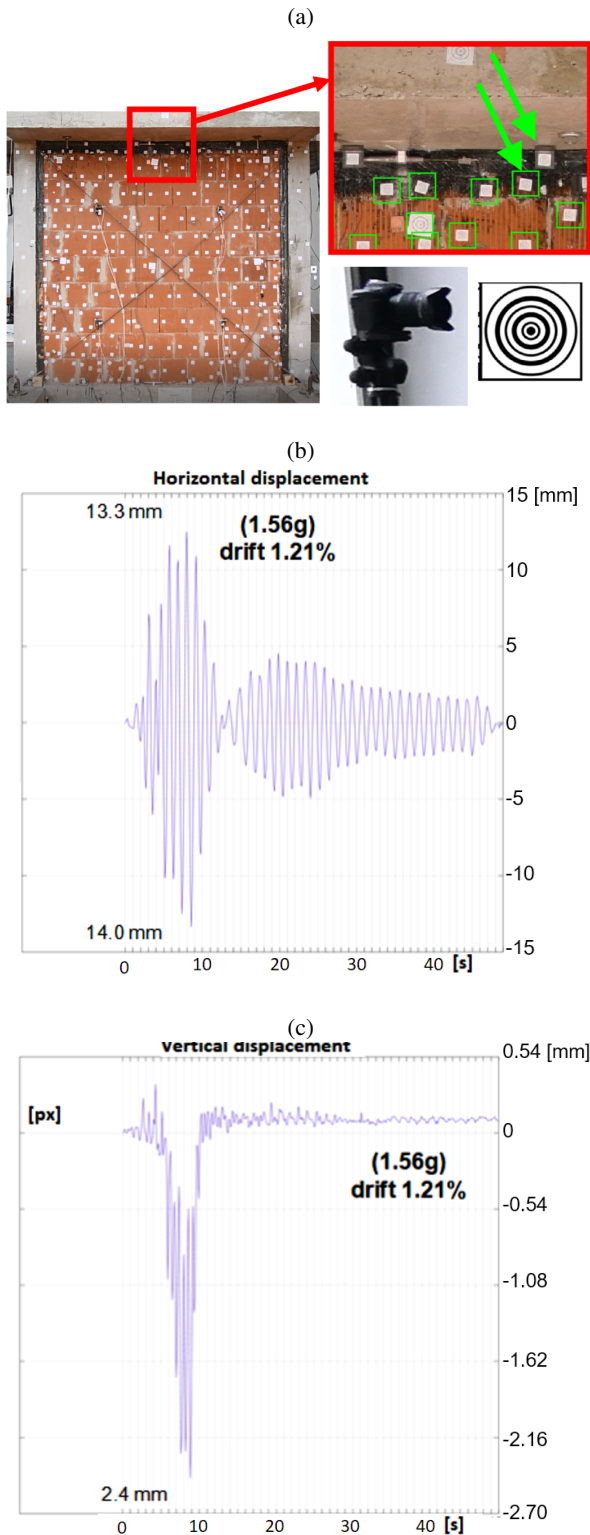


Fig. 14. DIC CivEng Vision results determined for PUFJ working in phase 1 between an RC frame and masonry infill B. DIC markers taken for analysis (green arrows) and a photo camera (a), acquired changes of: horizontal displacement (b) and vertical displacement (c)

like excitation is visible. The maximum horizontal relative displacements range between -14.0 mm and -13.3 mm. This corresponds to the shear angle of 70% in the flexible joint of

20 mm in thickness, denoting the high potential for dissipating deformation energy while maintaining contact. Such high shear deformation, detected on the RC frame-infill wall interface, confirms high efficiency of PUFJ in transferring high loads and high deformations simultaneously. Moreover, the DIC method seems to be the proper tool for monitoring large deformations in flexible bonding of elements undergoing dynamic action.

In the vertical graph (Fig. 14c), the tearing process is visible from the maximum vertical displacement of 2.4 mm (linear strain of 12%), observed in PUFJ. After that, no effort was observed in PUFJ in the vertical direction when the integrity of infill B was lost in phase 1.

6. DISCUSSION

The above-presented dynamic diagnosis tool, with the inertance function as the background, might prove useful in the monitoring of changes in the structural condition of various historical masonry buildings. This advanced tool allows investigators to obtain solidly based information about the structural condition of assessed structures. The use of a modal hammer and accelerometers with acquisition and a modal analysis system is not complicated. In addition, application of this system on historical objects of poor structural condition is easy and safe, because the required dynamic excitation (with a modal hammer) is very low and should not cause harmful consequences to the damaged structure, while other dynamic excitations might do so. Moreover, accessibility of this method in the assessment of various parts of objects is practically unconstrained. It renders the inertance analysis system a suitable diagnostic and monitoring tool, omitting the disadvantages of traditionally used methods with ambient vibrations (e.g. dynamic excitation of a structure with a vibrating machine put on a soil surface, or a harmonic shaker installed on an investigated structure). The inertance function method additionally offers a wide band of the analysis frequency domain, independent from the excitation source.

Knowledge about structural stiffness change makes for crucial information required by engineers during inspections. A classic and very popular monitoring system, used widely around the world – i.e. gypsum plasters installed on cracks – is unable to provide a deep understanding of the structural condition of an investigated object. It provides only simple information in a 0/1 mode (cracked/not cracked), which is not enough for assessment of the structural condition of historical buildings, especially in seismic areas. Also, other classical methods of damage evaluation, such as crack width sensors, are unable to predict common structural stiffness changes, thus numerical analysis has to be applied. It is known that changes of the structural condition (stiffness), after damage occurrence or repair, can cause a shift of natural frequencies in the structure. In some cases, the frequencies can be shifted to the dangerous frequency zone, if they are in resonance with dominant frequencies of an earthquake excitation [3].

Detection of stiffness changes and structural deterioration is very important not only in seismic areas, which was shown by the collapse of the Pavia Tower in the past [10]. The pro-

posed tool with the inertance function analysis is more versatile and offers more critical structural information in comparison to classical methods, which require further elaborations to conclude structural integrity. This is the case mainly in the detection of structural deterioration of materials, influencing changes in strength, stiffness and safety exploitation of structures, especially old historical masonry ones.

Even though Fourier transform and digital image correlation require the same or similar effort in terms of numerical analysis, the equipment being used offers different opportunities of their application. Digital image correlation offers huge flexibility in terms of indirectly measured physical values of a certain object and measured area, but requires specific light and test setup. On the other hand, traditional accelerometers are almost plug and measure, but they limit the results only to the measured point.

The general conclusion is that all above-presented methodologies are reliable enough when implemented correctly. Therefore, they may provide cross-check framework to upgrade reliability in the cases of composite structures with different materials involved (RC members – brick infills-PUFJ) with different mechanical responses and interfaces as well as with variation of damages in severity and location that may require global-local-sensitive methods. The obtained experimental physical quantities or dynamic characteristics can be further used in the numerical analyses needed or in simulations, to validate advanced models and deepen our understanding of complex structural behavior.

7. CONCLUSIONS

The inertance function method presented herein appears to be a proper diagnostic tool for simple experimental modal analysis of real structures and their structural elements, where detection of changes in the structural condition and dynamic properties is required, also as a non-destructive testing and monitoring method. It is characterized by:

- high efficiency in analysis of dynamic properties of large-scale structures and in monitoring their changes caused by damage and repair processes;
- wide range of information generated useful for engineers;
- simplicity of use – not requiring very expensive or difficult-in-transportation equipment;
- safety of application on weak structures and structural elements of poor quality.

The unique shake table tests carried out confirmed that the PUFJ solution can be effectively evaluated and monitored using the alternative methods. They proved that the inertance method and digital image correlation provide reliable results, comparable to other classical methods.

The different methods confirmed that the seismic joints – either resin-injected PUFJ used as a seismic protection method in existing structures, or prefabricated PUFJ used in the construction of new infills as a combined thermal-seismic retrofit technique – protected the brick infilled RC structure in an efficient manner. The dynamic characteristics' assessment proved both seismic joint types provided equivalent efficiency in delaying severe damage accumulation on the infill wall and the rate

of damage accumulation for multiple test runs. Furthermore, the DIC method validated the unique shear deformation and bond performance of the PUFJ joints in both types of injected or prefabricated joints as the key parameter.

ACKNOWLEDGEMENTS

This research activity was performed within the framework of the project entitled Seismology and Earthquake Engineering Research Infrastructure Alliance for Europe – SERA, INFills and MASONry structures protected by deformable POLyurethanes in seismic areas (INMASPOL). The project leading to this application has received funding from the European Union's Horizon 2020 research and innovation program under grant agreement No. 730900.

REFERENCES

- [1] M. Hejazi, "Bam Citadel after the Earthquake," in *Structural Analysis of Historical Constructions (SAHC)*, New Delhi, 2006, pp. 199–208.
- [2] M. Saatcioglu *et al.*, "The August 17, 1999, Kocaeli (Turkey) earthquake – damage to structures," *Can. J. Civ. Eng.*, vol. 28, pp. 715–737, 2001.
- [3] T. Rousakis *et al.*, "Flexible joints between RC frames and masonry infill for improved seismic performance – shake table tests," in *Brick and Block Masonry – From Historical to Sustainable Masonry*, 1st ed., J. Kubica, A. Kwiecień, and Ł. Bednarz, Eds. CRC Press, 2020, pp. 499–507, doi: [10.1201/9781003098508-68](https://doi.org/10.1201/9781003098508-68).
- [4] A. Kwiecień, "Polymer flexible joints An innovative repair system protecting cracked masonries against stress concentrations," in *Protection of Historical Buildings PROHITECH'09*, Italy, Jun. 2009, pp. 1033–1038.
- [5] J. Jasiński, A. Kwiecień, and M. Skłodowski, "New flexible intervention solutions for protection, strengthening and reconstruction of damaged heritage buildings," in *International Conference on Earthquake Engineering and Post Disaster Reconstruction Planning (ICEE-PDRP 2016)*, Nepal, Apr. 2016, pp. 304–313.
- [6] A.I. Karabinis, A.D. Baltzopoulou, and T.C. Rousakis, "The earthquake of Lefkas 14/8/2003. Investigation of seismic vulnerability of structures (in Greek)," in *15th Concrete Conference (TCG)*, Alexandroupolis, Greece, Oct. 2006, vol. B, pp. 330–339.
- [7] A.I. Karabinis and T.C. Rousakis, "Evaluation of RVS method for pre-seismic assessment of structures utilizing post-earthquake damage investigations," in *Urban habitat constructions under catastrophic events: COST action C26; proceedings of the final conference*, F.M. Mazzolani, Ed. Boca Raton: CRC Press, 2010, pp. 589–600. [Online]. Available: <https://www.routledge.com/Urban-Habitat-Constructions-Under-Catastrophic-Events-Proceedings-of-the-Mazzolani/p/book/9780415606851>.
- [8] M. Tapan, M. Comert, C. Demir, Y. Sayan, K. Orakcal, and A. Ilki, "Failures of structures during the October 23, 2011 Tabanlı(Van) and November 9, 2011 Edremit (Van) earthquakes in Turkey," *Eng. Fail. Anal.*, vol. 34, pp. 606–628, Dec. 2013, doi: [10.1016/j.engfailanal.2013.02.013](https://doi.org/10.1016/j.engfailanal.2013.02.013).

- [9] K. Flaga and A. Kwiecień, "Efficiency of CFRP Strengthening of Arches Tested by Failure of Historical Building after the Inappropriate Repair Intervention," *Adv. Mater. Res.*, vol. 133–134, pp. 837–842, Oct. 2010, doi: [10.4028/www.scientific.net/AMR.133-134.837](https://doi.org/10.4028/www.scientific.net/AMR.133-134.837).
- [10] L. Binda, A. Anzani, and A.E. Saisi, "Failures due to long term behaviour of heavy structures: the Pavia Civic Tower and the Noto Cathedral," *WIT Trans. Built Environ.*, vol. 66, pp. 99–108, 2003.
- [11] D. Bajno, L. Bednarz, Z. Matkowski, and K. Raszczuk, "Monitoring of Thermal and Moisture Processes in Various Types of External Historical Walls," *Materials*, vol. 13, no. 3, p. 505, Jan. 2020, doi: [10.3390/ma13030505](https://doi.org/10.3390/ma13030505).
- [12] D. Bajno, Ł. Bednarz, and T. Nowak, "Problems Relating to Assessment, Repair and Restoration of Wooden Roof Structures in Historic Buildings, as Exemplified by Two Case Studies in Southern Poland," *Adv. Mater. Res.*, vol. 778, pp. 888–894, Sep. 2013, doi: [10.4028/www.scientific.net/AMR.778.888](https://doi.org/10.4028/www.scientific.net/AMR.778.888).
- [13] J. Jasieńko, T. Nowak, and Ł. Bednarz, "Wrocław University's Leopoldinum Auditorium – Tests of Its Ceiling and a Conservation and Strengthening Concept," *Adv. Mater. Res.*, vol. 133–134, pp. 265–270, Oct. 2010, doi: [10.4028/www.scientific.net/AMR.133-134.265](https://doi.org/10.4028/www.scientific.net/AMR.133-134.265).
- [14] L. Bednarz, D. Bajno, Z. Matkowski, I. Skrzypczak, and A. Leśniak, "Elements of Pathway for Quick and Reliable Health Monitoring of Concrete Behavior in Cable Post-Tensioned Concrete Girders," *Materials*, vol. 14, no. 6, p. 1503, Mar. 2021, doi: [10.3390/ma14061503](https://doi.org/10.3390/ma14061503).
- [15] A. Kwiecień, J. Chelmecki, and P. Matysek, "Non-destructive test of brick masonry columns using change in frequency and inertance response," in *Structural Analysis of Historical Constructions (SAHC)*, Poland, 2012, pp. 2437–2444.
- [16] J. Chelmecki, A. Kwiecień, and B. Zając, "The inertance function in dynamic diagnosis of undamaged and damaged structures," *Tech. Trans. Environ. Eng.*, vol. 110, no. 1-Ś, pp. 3–12, 2013.
- [17] A. Kwiecień, B. Zając, and J. Chelmecki, "Dynamic testing of anti-vibration protection constructed in floor topping of historic masonry building," in *9th International Conference on Structural Dynamics, EURO-DYN 2014*, Portugal, Jul. 2014, pp. 907–912.
- [18] A. Kwiecień, "Flexible polymer adhesives versus stiff mineral and epoxy adhesives tested dynamically on masonry columns strengthened using of bonded GFRP mesh," in *8th International Conference on Structural Dynamics, EURO-DYN 2011*, Belgium, Jul. 2011, pp. 3258–3264.
- [19] T. Rousakis, V. Vanián, T. Fanaradelli, and E. Anagnostou, "3D FEA of Infilled RC Framed Structures Protected by Seismic Joints and FRP Jackets," *Appl. Sci.*, vol. 11, no. 14, p. 6403, Jul. 2021, doi: [10.3390/app11146403](https://doi.org/10.3390/app11146403).
- [20] T. Rousakis, E. Anagnostou, and T. Fanaradelli, "Advanced Composite Retrofit of RC Columns and Frames with Prior Damages – Pseudodynamic Finite Element Analyses and Design Approaches," *Fibers*, vol. 9, no. 9, p. 56, Sep. 2021, doi: [10.3390/fib9090056](https://doi.org/10.3390/fib9090056).
- [21] A. Kwiecień, "Reduction of stress concentration by polymer flexible joints in seismic protection of masonry infill walls in RC frames," *IOP Conf. Ser. Mater. Sci. Eng.*, vol. 474, p. 012003, Feb. 2019, doi: [10.1088/1757-899X/474/1/012003](https://doi.org/10.1088/1757-899X/474/1/012003).
- [22] A. Viskovic, L. Zuccarino, A. Kwiecień, B. Zając, and M. Gams, "Quick Seismic Protection of Weak Masonry Infilling in Filled Framed Structures Using Flexible Joints," *Key Eng. Mater.*, vol. 747, pp. 628–637, Jul. 2017, doi: [10.4028/www.scientific.net/KEM.747.628](https://doi.org/10.4028/www.scientific.net/KEM.747.628).
- [23] T. Rousakis *et al.*, "Deformable Polyurethane Joints and Fibre Grids for Resilient Seismic Performance of Reinforced Concrete Frames with Orthoblock Brick Infills," *Polymers*, vol. 12, no. 12, p. 2869, Nov. 2020, doi: [10.3390/polym12122869](https://doi.org/10.3390/polym12122869).
- [24] A. Kwiecień and P. Kubon, "Dynamic Analysis of Damaged Masonry Building Repaired with the Flexible Joint Method / Analiza Dynamiczna Uszkodzonego Murowanego Budynku Naprawionego z Zastosowaniem Polimerowego Złącza Podatnego," *Arch. Civ. Eng.*, vol. 58, no. 1, pp. 39–55, Mar. 2012, doi: [10.2478/v.10169-012-0003-2](https://doi.org/10.2478/v.10169-012-0003-2).
- [25] A. Kwiecień *et al.*, "PUFJ and FRPU earthquake protection of infills tested in resonance," in *1st Croatian Conference on Earthquake Engineering (1CroCEE)*, Croatia, Mar. 2021, pp. 465–475.
- [26] M. Tekieli, S. De Santis, G. de Felice, A. Kwiecień, and F. Roscini, "Application of Digital Image Correlation to composite reinforcements testing," *Compos. Struct.*, vol. 160, pp. 670–688, Jan. 2017, doi: [10.1016/j.compstruct.2016.10.096](https://doi.org/10.1016/j.compstruct.2016.10.096).